

Nucleosynthesis of elements between Sr and Ag in neutron- and proton-rich neutrino-driven winds

A. Arcones

Institut für Kernphysik, Technische Universität Darmstadt, Schlossgartenstraße 2,
D-64289 Darmstadt, Germany

GSI Helmholtzzentrum für Schwerionenforschung GmbH, Planckstr. 1 D-64291
Darmstadt, Germany

E-mail: almudena.arcones@physik.tu-darmstadt.de

J. Bliss

Institut für Kernphysik, Technische Universität Darmstadt, Schlossgartenstraße 2,
D-64289 Darmstadt, Germany

Abstract. Neutrino-driven winds that follow core collapse supernovae were thought to be the site where half of the heavy elements are produced by the r-process. Although recent hydrodynamic simulations show that the conditions in the wind are not enough for the r-process, lighter heavy elements like Sr, Y, and Zr can be produced. However, it is still not clear whether the conditions in the wind are slightly neutron rich or proton rich. Here we investigate the nucleosynthesis in neutrino-driven winds for both these conditions and systematically explore the impact of wind parameters on abundances. Our results show the difficulty of obtaining a robust abundance pattern in neutron-rich winds where also an over production of Sr, Y, and Zr is likely. In proton-rich conditions, the abundances smoothly change when varying wind parameters. Constraints for wind parameters and neutrino energies and luminosities will soon become available by combining nucleosynthesis studies, like the one presented here, with new and future experimental data and observations.

Submitted to: *J. Phys. G: Nucl. Phys.*

1. Introduction

Which elements heavier than iron are synthesized in neutrino-driven winds? Half of the nuclei heavier than iron are produced by the r-process (rapid neutron capture process). This is characterized by very fast neutron captures compared to beta decays and thus by the production of extreme neutron-rich nuclei that eventually decay to stability (for a review see [9]). The neutrino-driven winds that develop after successful supernova explosions [12] were suggested as the site of the r-process [32, 58]. The very neutron-rich and explosive conditions required by this process point to core-collapse supernovae, neutron star mergers [27, 17], and accretion disks [45]. In addition, the number of these events times the amount of r-process material produced by them has to account for the r-process isotopes in the solar system and in the oldest observed stars [44]. All this suggested that supernovae are the best candidate and triggered lot of investigations to understand neutrino-driven winds. However, the most recent and detailed studies indicate that neutrino-driven winds do not get enough neutron-rich conditions to produce elements up to uranium [4, 5, 25, 15, 43].

Even if not every supernova produces r-process elements, neutrino-driven winds remain an exciting astrophysical site for the nucleosynthesis of elements beyond iron and up to silver. First nucleosynthesis calculations based on hydrodynamic simulations [57] showed that the seed nuclei (that capture neutrons during the r-process) in neutrino-driven winds are heavier than iron-group elements. The nucleosynthesis in the wind starts with an alpha-rich freeze-out and continues with charged particle reactions and neutron captures. When the temperature drops only the latter can continue towards heavy nuclei via the r-process [57]. However, the charged particle reactions or alpha process already synthesizes elements up to $N = 50$ and $A = 90$.

There are at least two indications that further studies are necessary to understand the origin of elements between Sr and Ag. First, observations of very old stars [44] indicate that there is more than one r-process: one produces a robust pattern and gets up to uranium, another one contributes only to the lighter heavy elements (Sr to Ag). Qian & Wasserburg showed that neutrino driven winds can be the site producing these elements [36, 37, 38]. Moreover, the solar system abundances for these lighter heavy elements cannot be explained only with the r- and s-process as shown by [49, 33]. The missing contribution can correspond to charged particle reactions in the neutrino-driven winds [7, 13] but also to fast rotating stars at low metallicities (see [18] and references therein). The process that contributes to the production of elements between Sr and Ag can be the LEPP (lighter element primary process [49]), a low metallicity s-process [18] or charged particle reactions [36] combined with a weak r-process [50] and/or the νp -process [35, 19, 55].

The elements between Sr and Ag in neutrino-driven winds can be used to understand better neutrino-driven winds and supernovae, if we combine nucleosynthesis calculations (including the most recent experimental data) and observations of very old stars. In contrast to the r-process (for which many questions remain open

concerning the astrophysical site and the nuclear properties of the nuclei involved) for the production of lighter heavy elements in neutrino-driven winds we have (or will have soon) enough information to explain their origin and use them to learn about the astrophysical conditions. There are three reasons for this positive statement: 1) the required astrophysical conditions to produce elements up to Ag are found in current hydrodynamic simulations, 2) the still unmeasured experimental data necessary for the nucleosynthesis calculations will be accessible in new radioactive beam facilities because most of the nuclei involved are relatively close to stability, 3) present and planned surveys are rapidly improving in quality and quantity allowing to collect more information about very old stars that provide a unique fingerprint of early nucleosynthesis. All these advances required a parallel effort with nucleosynthesis studies. In this paper we use a trajectory from [4] and varying the wind parameters to study the production of elements between Sr and Ag. This was analyzed in previous works based on a full-consistent supernova simulation [53], full parametric high-entropy wind models [13], and simplified wind simulations [43, 7]. Our work complement these previous studies giving a broader and more systematic overview of the production of lighter heavy elements and wind parameters.

In this paper, we briefly review the nucleosynthesis occurring in neutrino-driven winds in Sect. 2 and we introduce the trajectory and the nucleosynthesis network in Sect. 3. The results are divided into neutron-rich winds (Sect. 4) and proton-rich winds (Sect. 5). The summary and conclusions are in Sect. 6.

2. Wind nucleosynthesis

The nucleosynthesis processes occurring in neutrino-driven winds are primary processes, i.e., they start from neutrons and protons and not from existing seed nuclei. In the outer layers of the neutron star temperature and density are high and the composition is dominated by nucleons, although light cluster (^2H , ^3H , ^3He , ^4He) can also be present (see e.g. [6]). This matter gets ejected after absorbing enough energy from neutrinos that are emitted during the cooling of the neutron star [12]. As matter is ejected its temperature and density drop and this allows nuclear reactions to start building alpha particles and seed nuclei. The composition of the seed distribution and the subsequent evolution towards synthesizing elements beyond the iron group depend on three wind quantities (see e.g., [31, 39, 23, 48]): entropy, expansion time scale, and electron fraction. These parameters determine the ratio between nucleons and seed nuclei: neutron-to-seed (Y_n/Y_{seed}) and proton-to-seed (Y_p/Y_{seed}) ratios. Depending on the value of these ratios at temperatures around 3 GK, three processes are possible: 1) r-process [23, 16, 48] if $Y_n/Y_{\text{seed}} \gtrsim 100$, 2) weak r-process [50] if $Y_n/Y_{\text{seed}} \sim 1$, and 3) νp -process [35, 19, 55] if Y_n/Y_{seed} is very small and $Y_p > Y_n$, i.e., proton-rich conditions.

How the wind parameters affect the neutron-to-seed ratio has been extensively studied in the context of the r-process, see e.g. [31, 23]. The *entropy* in radiation-dominated environments depends on temperature and density: $S \propto T^3/\rho$. Therefore,

high entropy is achieved at high temperatures and low densities and favors high neutron-to-seed ratios. High temperature implies energetic photons that destroy the seed nuclei into nucleons, thus reducing Y_{seed} and increasing Y_n . In addition the formation of seed nuclei starts with three body reactions: $3\alpha \rightarrow {}^{12}\text{C}$ and ${}^4\text{He} (\alpha n, \gamma) {}^9\text{Be} (\alpha, n) {}^{12}\text{C}$. At low density the probability that these reactions occur is small and this results in lower Y_{seed} . The *expansion time scale* indicates how fast matter expands during the alpha and seed formation at temperature around 0.5 MeV: $\tau = \frac{r}{v}|_{T=0.5\text{MeV}}$ [39], with r and v being radius and velocity, respectively. If the expansion is very fast (i.e., small τ), the three body reactions do not have enough time to synthesize seed nuclei and Y_{seed} stays low. The *electron fraction* or electron abundance tells us if the wind is neutron rich ($Y_e < 0.5$) or proton rich ($Y_e > 0.5$). Since the environment is charge neutral the abundance of electrons is equal to the abundance of protons (free and in bound nuclei): $Y_e = \sum_i Z_i Y_i$ with Z_i the proton number of nucleus i and Y_i its abundance. In order to calculate the wind nucleosynthesis one needs the electron fraction at high temperatures ($T \sim 10$ GK) when the matter is still in nuclear statistical equilibrium and the composition consists mainly of neutrons and protons. Under such conditions $Y_e = Y_p/(Y_p + Y_n)$. The subsequent evolution of Y_e is done within the nucleosynthesis network (Sect. 3) where weak reactions are included. If the electron fraction is very low $Y_e \lesssim 0.3$ the neutron-to-seed ratio will be high enough for the r-process to occur. If $0.4 \lesssim Y_e \lesssim 0.5$ only a weak r-process is possible unless the entropy is very high and/or the expansion time scale very short. For $Y_e > 0.5$ the νp -process occurs if enough neutrons can be produced by antineutrino absorption on protons. Here we will ignore the r-process because there are already numerous studies about wind parameters and r-process and current hydrodynamic supernova simulations show that extreme neutron-rich conditions are not found in general (see [9, 8] and references therein). Our focus here is on the weak r-process (Sect. 4) and the νp -process (Sect. 5), both can occur based on current models and produce heavy elements between Sr and Ag.

3. Astrophysical conditions and nucleosynthesis network

The evolution of wind trajectories varies for different progenitors, explosion energy, anisotropic evolution of the explosion, and during time after the explosion (see e.g., [4, 3, 15, 43]). Therefore, a complete picture of the nucleosynthesis from neutrino-driven winds requires a large number of three-dimensional simulations following the explosion and the wind evolution during few seconds and for different progenitors. This is far from being possible because of the huge computational time necessary and also due to the still uncertain details of the explosion [26, 10] and wind evolution [8]. Among these uncertainties are the neutrino matter interactions on the surface of the neutron star [41, 42, 28], neutrino oscillations [29, 11], rotation and magnetic fields [46, 47, 30]. In view of these open questions and uncertainties our strategy here is to explore the impact of the wind parameters (Sect 2) using a single trajectory and varying its entropy, expansion timescale and initial electron fraction. This cannot determine the integrated

nucleosynthesis from neutrino-driven winds but helps to understand the dependencies of abundances and wind parameters as well as to suggest possible constraints based on observations (see e.g. [7, 51]) and chemical evolution [20].

The trajectory used in our investigation corresponds to the explosion model M1511r1 presented in [4] and it is ejected 5 s after bounce. This simulation has a simple but very efficient neutrino transport that allows to study the evolution of the wind for various progenitors in one and two dimensions [4, 3]. The evolutions of the density and temperature for the trajectory are shown in Fig. 1. In the neutrino-driven wind, matter expands very fast as indicated by the rapid initial drop of density and temperature ($t \lesssim 0.1$ s). The wind moves through and collides with the early, slow-moving supernova ejecta. The result is a reverse shock where kinetic energy is transformed into internal energy producing an increase of temperature and density (see [4] for more details about the reverse shock). The evolution after the reverse shock is significantly slower and matter can maintain almost constant thermodynamic conditions during half a second or even longer. However, the details of the evolution after the reverse shock strongly depend on the pressure distribution of the slow supernova ejecta and this is affected by multidimensional evolution during the explosion (see [3] for more details).

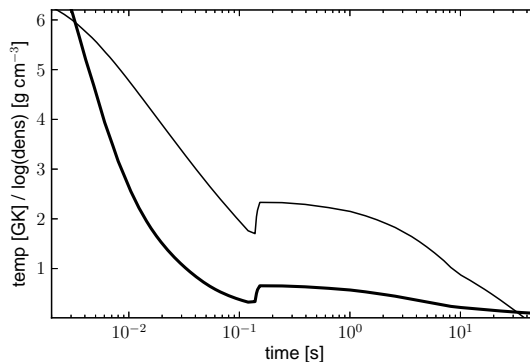


Figure 1. Evolution of the temperature (thin line) and the logarithmic of the density (thick line) for the trajectory ejected 5 s after bounce of the model M1511r1 [4]. The reverse shock produces the jump between 0.1 s and 0.2 s.

The trajectory has the following wind parameters: $S_{\text{wind}} = 78k_{\text{B}}/\text{nuc}$, $\tau = 5$ ms, and $Y_e = 0.484$. These values are within the typical values obtained in different hydrodynamic simulations [4, 54, 3, 15, 43, 41]. We employ this trajectory as reference case and vary the parameters to cover typical conditions values found in wind simulations. The entropy is decreased and increased by a 30% by changing the density as in a radiation dominated environment, $S \propto T^3/\rho$. The time scale is modified from 1 ms to 10 ms by using a factor over all the trajectory time. Finally the initial electron fraction is given as a network parameter and it is necessary to calculate the initial NSE composition. The following evolution of Y_e is performed within the network where we include neutrino reactions on nucleons. This implies that the neutrino luminosities and

energies (which are given also as network parameters) should be consistent with the electron fraction.

Each network calculation starts at a temperature of ~ 10 GK, thus assuming nuclear statistical equilibrium composition for a given initial Y_e . The evolution of the composition is followed using a full reaction network [19], which includes 4053 nuclei from H to Hf including both neutron- and proton-rich isotopes. Theoretical reaction rates are from the statistical code NON-SMOKER [40] and experimental rates are included [1] when available. The theoretical weak interaction rates are the same as in [19] and we use experimental beta-decay rates when available [34].

4. Neutron-rich winds

In slightly neutron-rich winds a weak r-process depends on wind parameters in the same way as the r-process occurring in very neutron-rich winds. However, there are two main differences between these two processes: 1) the weak r-process produces elements only below the second peak ($Z < 56$) in contrast to the r-process that can go up to uranium, 2) in the weak r-process matter moves towards higher Z via beta decays but mainly via (α, n) reactions [57], while in the r-process beta decay is the dominant reaction to change isotopic chain. In order to explore the behavior of the weak r-process we have varied the wind parameters and the resulting abundances are shown in Fig. 2. In general higher neutron-to-seed ratio (i.e., higher entropy, shorter expansion time scale, lower electron fraction) leads to heavier elements. Note that the green line, shown in the three panels, is the reference case and corresponds to unchanged entropy and expansion time scale and $Y_e = 0.45$.

In the top panel of Fig. 2 the entropy is increased (1.3 S) and decreased (0.7 S) by a 30% while the expansion time scale is unmodified and $Y_e = 0.45$. For the low entropy case there is a maximum around $Z = 40$ and strong odd-even effects below this element. The maximum corresponds to all stable Zirconium isotopes with ^{90}Zr and ^{94}Zr being the most abundant ones. Moreover, only the isotope ^{88}Sr is present in the final abundances for $Z = 38$. These two features clearly indicate that the path does not move up through stability but through unstable neutron-rich isotopes and eventually decays populating the stable isotopes reachable from the neutron-rich side. If the path would move only along stability, the final abundance would contain other Sr isotopes and ^{94}Zr would not be very abundant. Therefore, the maximum at $Z = 40$ is not directly linked to the shell closure at $N = 50$ for these conditions. The path gets to the neutron rich side until $N = 50$ and continues via beta decays and neutron captures increasing the proton number at constant neutron number $N = 50$ until ^{86}Kr is reached. This stable isotope does not beta decay allowing neutrons to be captured and the path to overcome the waiting point. Therefore, the peak around $Z = 40$ is indirectly linked to the magic number $N = 50$ in the sense that matter accumulates at ^{86}Kr but not at ^{88}Sr , ^{89}Y , and ^{90}Zr . Similar results were already discussed in [57].

With higher entropy additional neutron captures allow matter to flow further away

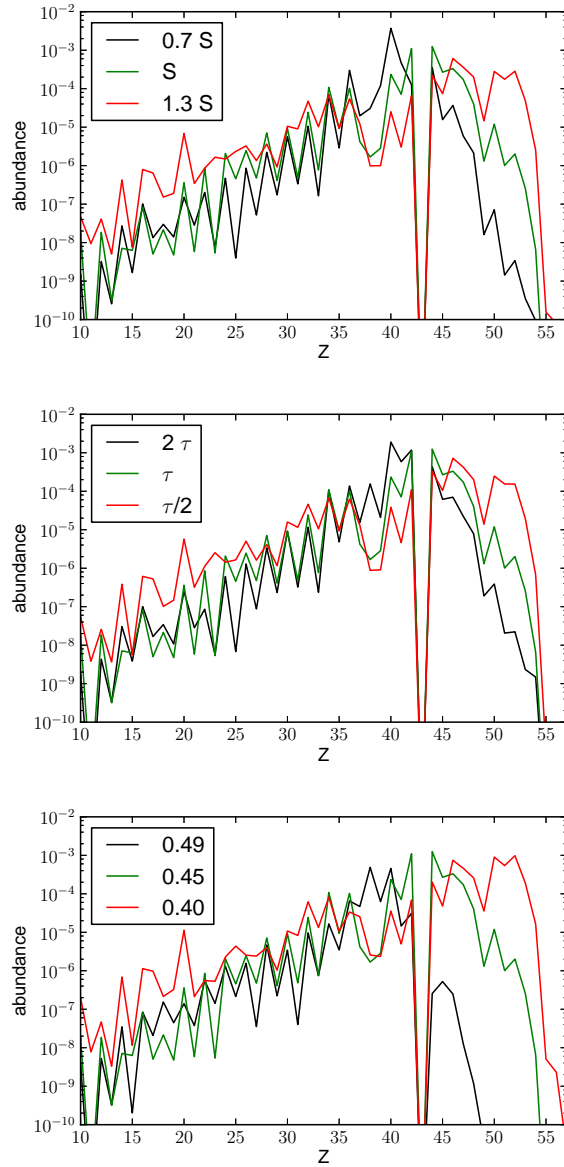


Figure 2. Elemental abundances after decay to stability showing the impact of entropy, expansion time scale and electron fraction, from the top to the bottom panel.

of stability and overcome the magic number $N = 50$ at lower Z . This flow only stops at the shell closure $N = 82$ and it is followed by beta decays and neutron captures, i.e. moves up in Z at constant N . Therefore, the final abundances have three features different to the low entropy case: lower abundances in the region of $36 < Z < 42$ (matter is moved from lower to higher Z), higher abundances for $Z > 43$, and an abrupt drop at $Z \sim 55$. In addition, there is a small maximum in the abundances between $50 < Z < 53$ that corresponds to mass numbers $118 < A < 130$. This matter reaches $N = 82$ and accumulates there before decaying to stability. The variations of the expansion time scale (middle panel, Fig. 2) and the electron fraction (bottom panel, Fig. 2) have a

similar impact to the changes in entropy.

Other important result is that any variation of the wind parameters changes significantly the abundance pattern. When the neutron-to-seed ratio increases there is not only a variation on the maximum Z that it is reached, but also the abundances are different for low Z . This may be relevant if one wants to compare to observations. Here, we are interested in the production of elements between Sr and Ag in neutrino-driven winds. In Fig. 2 one can see that these elements are very sensitive to the wind parameters. In order to get a better overview, Fig. 3 shows the abundances of Sr, Y, Zr, and Ag for various electron fractions and entropies (left column) and time scales (right column). For low neutron-to-seed ratio, i.e. at high Y_e , low entropy and long time scale, Sr, Y, and Zr dominate the composition. While for higher neutron-to-seed ratios silver is more abundant at expenses of Sr, Y, and Zr whose abundances are lower. An important feature are the structures in the panels for Sr, Y, and Zr. Their abundances oscillate and present several minima and maxima when wind parameters are varied. In contrast, the abundances of silver smoothly change with wind parameters. Observations [44] of the r-process indicate that the abundance pattern between Sr and Ag is not so robust as above $Z \approx 50$ (in stars with high enrichment of r-process). However, strong variations, as we find here, are also not expected. This could be an indication that the wind may not be neutron rich or that the wind parameters stays rather constant during the wind phase. However, this implies that all winds should have same entropy, expansion time scale, and electron fraction and current simulations show that the wind parameters change for different progenitors and at different times during the wind evolution. Other possibility is that the amount of neutron-rich material ejected is very small [53] and does not contribute to the observed abundances.

5. Proton-rich winds

When electron neutrinos and electron antineutrinos have similar energies the wind becomes proton-rich due to the neutron-proton mass difference. This can happen if neutral current reactions dominate in the region where neutrinos decouple from matter, i.e. at the neutrinosphere [25, 14]. Since the electron fraction of the wind is not yet well determined and there are simulations pointing to both neutron- and proton-rich conditions, we analyze now the nucleosynthesis in proton-rich winds.

In proton-rich conditions heavy elements are synthesized from seed nuclei via charged-particle reactions, i.e., (p, γ) , (α, γ) , (α, p) , and beta decays. These reactions allow the flow of matter to move on the proton-rich side of stability up to ^{64}Ge . This nucleus has a beta half life much longer than the expansion time scale of the wind, it is a bottleneck. However, the matter in the wind is exposed to high neutrino fluxes and the antineutrino absorption on protons produces neutrons that can be used to overcome such bottlenecks by (n, p) reactions. This is the νp -process that was first discussed by [35, 19, 55] and that depends on the neutron-to-seed ratio. Figure 4 shows the evolution of abundances for neutrons, protons, alpha particles, and seed nuclei. The neutron

abundance drops to very small values but still plays a key role in the synthesis of heavy elements via reactions such as (n, p) and (n, γ) .

The impact of the wind parameters on the νp -process has been already discussed by e.g. [35, 55]. Here we aim to give a more systematic overview with focus on the production of Sr, Y, Zr, and Ag. The reactions that control the production of heavy nuclei in proton-rich winds are the (n, p) reactions. Therefore, one needs to understand how the neutron-to-seed ratio changes with wind parameters. The amount of seeds (Y_{seed}) depends on entropy and time scale in the same way as in neutron-rich winds. Higher entropies and faster expansions lead to lower seed and higher neutron abundances, i.e. higher Y_n/Y_{seed} . The impact on the abundance of these two wind parameters and of Y_e is presented in Fig. 5.

As in neutron-rich winds, we have increased and decreased the entropy by a 30% while keeping the expansion time scale of the simulation and $Y_e = 0.60$ (top panel, Fig. 5). In the three cases, Sr, Y and Zr are produced although for the wind with lower entropy only in small amount. With higher entropy Ag and Pd can be also synthesized and if the entropy were even higher also heavier elements would appear. Here we keep the entropy variation within a 30% of the original values, for more extreme variation see [35].

The expansion time scale (middle panel, Fig. 5) has a moderate impact on the abundances. This time scale corresponds to the expansion of matter when alpha particles form and thus affects the seed production. However, the expansion during other phases of the evolution critically affects the nucleosynthesis in proton-rich winds. Heavy nuclei are synthesized via charged particle reactions; therefore, the time that the matter spends at high enough temperatures ($T \gtrsim 2\text{GK}$) is also important due to the Coulomb barrier. Moreover, neutrons are needed to overcome the bottlenecks, thus also the time matter is exposed to neutrinos becomes relevant. This was studied in [52, 2] by changing the temperature of the reverse shock and the time scale of the evolution afterwards. They found that there is an optimal temperature for the reverse shock to form heavy nuclei. When matter is decelerated by the reverse shock and kept at $T \sim 2\text{GK}$, heavier elements can be produced. If the temperature stays higher, photo-dissociation reactions prevent the flow of matter to reach heavy elements, matter stays in a NiCu cycle [2]. If the reverse shock is at much lower temperature or even absence (as it is the case of low mass progenitor explosions [54, 21]), the matter expands very fast and antineutrinos do not have enough time to produce the necessary amount of neutrons to overcome the bottlenecks. Therefore, the expansion time scale in proton-rich winds is important during the alpha formation and also during the νp -process. In the middle panel of Fig. 5, we have varied the overall evolution by dividing or multiplying the trajectory time by a given factor. This means that a faster expansion through the reduction of the time scale by a factor has two effects: 1) there are less alpha particles and seed nuclei and Y_n/Y_{seed} can become higher than in the reference case, 2) matter is exposed to the electron antineutrino flux during less time and this reduces the amount of protons that can be converted into neutrons with the result of lower Y_n . Therefore, one effect compensates

the other and the final result is small changes in the abundances for different time scales.

The electron fraction plays a very important role as it determines the amount of free neutrons. The neutron-to-seed ratio increases when the seed abundance decreases as we have discussed above, but also when the neutron abundances increases. The initial electron fraction gives the amount of proton as initially nucleons dominate the composition, i.e., $Y_p = Y_e$ and $Y_n = 1 - Y_e$. When matter expands and forms seed nuclei, neutrons are rapidly captured but also produced by antineutrino absorption on protons. Therefore, the abundance of neutrons reaches an equilibrium given by

$$\frac{dY_n}{dt} = \lambda_{\bar{\nu}_e} Y_p - \sum_{Z,A} N_n Y(Z,A) \langle \sigma v \rangle_{(Z,A)} = 0, \quad (1)$$

here $\lambda_{\bar{\nu}_e}$ is the electron antineutrino absorption rate and $\langle \sigma v \rangle_{(Z,A)}$ is the sum of neutron capture rates ((n, γ) and (n, p)) for nucleus (Z, A) . This expression indicates the dependence of the neutron abundances on the proton abundances and thus on the initial electron fraction:

$$N_n = \rho Y_n N_A = \frac{\lambda_{\bar{\nu}_e} Y_p}{\sum_{Z,A} Y(Z,A) \langle \sigma v \rangle_{(Z,A)}}, \quad (2)$$

where ρ is the density and N_A the Avogadro number. Eq. (2) shows that neutron abundance increases for higher Y_p and $\lambda_{\bar{\nu}_e}$. The first one depends on Y_e and its effect is visible in the bottom panel of Fig. 5: higher electron fraction significantly increases the abundances of Sr, Y, and Zr and allows to produce heavier elements. The antineutrino absorption rate depends on antineutrino energy ($\epsilon_{\bar{\nu}_e}$) and number luminosity ($L_{n,\bar{\nu}_e}$): $\lambda_{\bar{\nu}_e} = L_{n,\bar{\nu}_e} \sigma_{\bar{\nu}_e p} \propto L_{n,\bar{\nu}_e} \epsilon_{\bar{\nu}_e}^2$. Therefore, an increase of antineutrino luminosity and energy will have similar effect to the increase of Y_e , i.e. the production of heavy elements becomes more efficient.

After studying neutron- and proton-rich wind nucleosynthesis, we find two main differences in the final abundances. First, in proton-rich conditions the abundance pattern is homogeneous. Depending on the wind parameter the heaviest element that can be produced changes. However, the overall pattern remains similar as it can be seen in Fig. 6 where the abundance of Sr, Y, Zr, and Ag are shown (color contours) for a broad range of entropies and electron fractions. If we compare this figure to the left column in Fig. 3, the difference between neutron- and proton-rich conditions becomes clear. In proton-rich winds the abundances smoothly change when varying wind parameters, while in neutron rich conditions these variations are far from being smooth and linear.

The second difference is the total abundance of heavy nuclei ejected. In proton-rich conditions the amount of heavy nuclei created is significantly smaller ($Y_{\text{seed}} \lesssim 10^{-4}$) than in neutron-rich winds ($Y_{\text{seed}} \gtrsim 10^{-3}$). The ejecta of proton-rich winds consist mainly of protons and alpha particles, while for neutron-rich the main contribution are alpha particles. This can be relevant for calculating the supernova contribution to the solar system abundances. For example it was shown by [22] that there is a limit on the amount of matter that can be ejected by every supernova with given electron fraction ($Y_e \lesssim 0.47$) in order not to over produce elements like Sr, Y, and Zr.

6. Summary and conclusions

The nucleosynthesis studies of neutrino-driven winds combined with observations of chemical abundances can give important hints about supernova explosions and the origin of elements beyond iron. Although neutrino-driven winds have been extensively studied as the best candidate for the production of heavy elements by the r-process, recent simulations indicate that winds are in general not enough neutron rich to produce elements heavier than silver. The production and chemical evolution of elements between Sr and Ag remains an open question and the contribution of neutrino-driven winds can reveal new aspects about core-collapse supernova.

We have systematically studied the synthesis of lighter heavy elements (between Sr and Ag) in slightly neutron-rich ($Y_e < 0.5$) and proton-rich ($Y_e > 0.5$) winds. The nucleosynthesis in neutrino-driven winds depends on entropy, expansion time scale, and electron fraction. Therefore, we have varied all of these wind parameters and analyzed their impact on the abundances of lighter heavy elements. The entropy affects in a similar way for neutron- and proton-rich conditions: higher entropies allow for more free nucleons and less seed nuclei. This results in higher neutron-to-seed ratio that for both conditions triggers the production of heavier elements. The expansion time scale has the same effect as the entropy in neutron-rich winds: faster expansion reduces the amount of seed nuclei. However, for the νp -process a faster expansion not only means less seed nuclei but also less time that the matter is exposed to antineutrinos. The net result is less neutrons and less seed, therefore variations of the overall expansion time scale do not lead to large changes in abundances. The impact of the electron fraction has been discussed in previous works and we have summarized that in neutron-rich conditions lower Y_e and in proton-rich conditions higher Y_e lead to the formation of heavier elements.

In addition to the obvious difference in the isotopic composition, there are two other important differences between neutron- and proton-rich winds: the amount of matter ejected and the abundance pattern. These characteristics can be key when we compare to observations and study the contribution of supernova to the solar system abundances.

In proton-rich winds, most of the ejected matter consists of protons and alpha particles, while the amount of heavy nuclei is very small. In neutron-rich conditions, alpha particles also dominate but heavy nuclei are more abundant than in proton-rich conditions. Indeed if every neutrino-driven wind stays neutron-rich for several seconds, there would be an overproduction around $A = 90$ [22, 56]. This already implies that not every neutrino-driven wind can be neutron-rich. Note that for electron fractions very close to 0.5 the amount of heavy elements ejected is again very small. Therefore, one could constrain the neutron-richness assuming all winds are similar.

Other way of constraining the wind parameters is to compare the abundance obtained in our nucleosynthesis studies to observations of very old stars. There are several indications that the elements between Sr and Ag are produced by a different site or process than the heavier elements [36, 33]. The fingerprint of this may be on

stars with low enrichment of heavy r-process elements [24]. In these observations, there are small variations in the abundance pattern for the lighter heavy elements. When we calculate the nucleosynthesis for different wind parameters, we find that the pattern is rather robust for proton-rich conditions but it varies significantly for neutron-rich conditions. We have presented an overview of the dependency of the abundance of Sr, Y, Zr, and Ag on the wind parameters. While in proton-rich winds the abundance change smoothly when varying the wind parameters, in neutron-rich winds we find strong variations in the abundances for small changes in any of the wind parameters. Therefore, if the neutrino-driven wind is responsible for the observed abundances at low metallicities, neutron-rich conditions would not provide the robustness observed in the abundance pattern. This may suggest that the wind is not neutron or proton rich but a combination of both conditions.

In order to make stronger conclusions for the wind parameters and its neutron richness more nucleosynthesis studies, observations, and nuclear experiments are necessary. All these will be achieved in the near future. The nucleosynthesis processes (weak r-process and νp -process) keep the path close to stability, therefore the relevant experimental information can be obtained with future radioactive ion beam facilities. To this end further nucleosynthesis studies are required to explore the sensitivity of the still unmeasured nuclear properties and thus to motivate the most relevant experiments. From the observational perspective, further observations are necessary for more stars with low enrichment of heavy r-process elements as well as for more elements for the already observed low metallicity stars. Combining all this with nucleosynthesis studies based on more advanced supernova simulations and on parametric models, it will be possible to constrain the neutron richness of the neutrino-driven winds. Even if the conclusion were that no elements heavier than iron are produced in core-collapse supernova, this will already strongly limit the wind parameters and the neutrino energies and luminosities. We are about to be able to use observations and nucleosynthesis studies, like the one presented here, to learn more about supernova explosions and neutrino-driven winds.

Acknowledgments

This work was funded by the Helmholtz-University Young Investigator grant No. VH-NG-825. The authors acknowledge support to EuroGENESIS, a collaborative research program of the European Science Foundation (ESF).

References

- [1] C. Angulo, et al. *Nucl. Phys. A*, 656:3–183, 1999.
- [2] A. Arcones, C. Fröhlich, and G. Martínez-Pinedo. *ApJ*, 750:18, 2012.
- [3] A. Arcones and H.-T. Janka. *A&A*, 526:A160, 2011.
- [4] A. Arcones, H.-T. Janka, and L. Scheek. *A&A*, 467:1227–1248, 2007.
- [5] A. Arcones and G. Martínez-Pinedo. *Phys. Rev. C*, 83(4):045809, 2011.

- [6] A. Arcones, G. Martínez-Pinedo, E. O'Connor, A. Schwenk, H.-T. Janka, C. J. Horowitz, and K. Langanke. *Phys. Rev. C*, 78(1):015806, 2008.
- [7] A. Arcones and F. Montes. *ApJ*, 731:5, 2011.
- [8] A. Arcones and F.-K. Thielemann. *Journal of Physics G Nuclear Physics*, 40(1):013201, 2013.
- [9] M. Arnould, S. Goriely, and K. Takahashi. *Phys. Repts.*, 450:97–213, 2007.
- [10] A. Burrows. *Reviews of Modern Physics*, 85:245–261, 2013.
- [11] H. Duan, A. Friedland, G. C. McLaughlin, and R. Surman. *Journal of Physics G Nuclear Physics*, 38(3):035201, 2011.
- [12] R. C. Duncan, S. L. Shapiro, and I. Wasserman. *ApJ*, 309:141–160, 1986.
- [13] K. Farouqi, K.-L. Kratz, B. Pfeiffer, T. Rauscher, F.-K. Thielemann, and J. W. Truran. *ApJ*, 712:1359–1377, 2010.
- [14] T. Fischer, G. Martínez-Pinedo, M. Hempel, and M. Liebendörfer. *Phys. Rev. D*, 85(8):083003, 2012.
- [15] T. Fischer, S. C. Whitehouse, A. Mezzacappa, F.-K. Thielemann, and M. Liebendörfer. *A&A*, 517:A80, 2010.
- [16] C. Freiburghaus, J.-F. Rembges, T. Rauscher, E. Kolbe, F.-K. Thielemann, K.-L. Kratz, B. Pfeiffer, and J. J. Cowan. *ApJ*, 516:381–398, 1999.
- [17] C. Freiburghaus, S. Rosswog, and F.-K. Thielemann. *ApJ*, 525:L121–L124, 1999.
- [18] U. Frischknecht, R. Hirschi, and F.-K. Thielemann. *A&A*, 538:L2, 2012.
- [19] C. Fröhlich, G. Martínez-Pinedo, M. Liebendörfer, F.-K. Thielemann, E. Bravo, W. R. Hix, K. Langanke, and N. T. Zinner. *Phys. Rev. Lett.*, 96(14):142502–+, 2006.
- [20] C. J. Hansen, M. Bergemann, G. Cescutti, P. François, A. Arcones, A. I. Karakas, K. Lind, and C. Chiappini. *A&A*, 551:A57, 2013.
- [21] R. D. Hoffman, B. Müller, and H.-T. Janka. *ApJL*, 676:L127–L130, 2008.
- [22] R. D. Hoffman, S. E. Woosley, G. M. Fuller, and B. S. Meyer. *ApJ*, 460:478–488, 1996.
- [23] R. D. Hoffman, S. E. Woosley, and Y.-Z. Qian. *ApJ*, 482:951–962, 1997.
- [24] S. Honda, W. Aoki, Y. Ishimaru, S. Wanajo, and S. G. Ryan. *ApJ*, 643:1180–1189, 2006.
- [25] L. Hüdepohl, B. Müller, H.-T. Janka, A. Marek, and G. G. Raffelt. *Phys. Rev. Lett.*, 104(25):251101, 2010.
- [26] H.-T. Janka. *Ann. Rev. Astron. & Astrophys.*, 62:407–451, 2012.
- [27] J. M. Lattimer, F. Mackie, D. G. Ravenhall, and D. N. Schramm. *ApJ*, 213:225–233, 1977.
- [28] G. Martínez-Pinedo, T. Fischer, A. Lohs, and L. Huther. *Phys. Rev. Lett.*, 109(25):251104, 2012.
- [29] G. C. McLaughlin, J. M. Fetter, A. B. Balantekin, and G. M. Fuller. *Phys. Rev. C*, 59:2873–2887, 1999.
- [30] B. D. Metzger, T. A. Thompson, and E. Quataert. *ApJ*, 659:561–579, 2007.
- [31] B. S. Meyer. *Phys. Rep.*, 227:257–267, 1993.
- [32] B. S. Meyer, G. J. Mathews, W. M. Howard, S. E. Woosley, and R. D. Hoffman. *ApJ*, 399:656–664, 1992.
- [33] F. Montes, T. C. Beers, J. Cowan, T. Elliot, K. Farouqi, R. Gallino, M. Heil, K.-L. Kratz, B. Pfeiffer, M. Pignatari, and H. Schatz. *ApJ*, 671:1685–1695, 2007.
- [34] NuDat2. "National Nuclear Data Center, information extracted from the NuDat 2 database".
- [35] J. Pruet, R. D. Hoffman, S. E. Woosley, H.-T. Janka, and R. Buras. *ApJ*, 644:1028–1039, 2006.
- [36] Y.-Z. Qian and G. J. Wasserburg. *ApJ*, 559:925–941, 2001.
- [37] Y.-Z. Qian and G. J. Wasserburg. *Phys. Rep.*, 442:237–268, 2007.
- [38] Y.-Z. Qian and G. J. Wasserburg. *ApJ*, 687:272–286, 2008.
- [39] Y.-Z. Qian and S. E. Woosley. *ApJ*, 471:331–351, 1996.
- [40] T. Rauscher and F.-K. Thielemann. *At. Data Nucl. Data Tables*, 75:1–352, 2000.
- [41] L. F. Roberts. *ApJ*, 755:126, 2012.
- [42] L. F. Roberts, S. Reddy, and G. Shen. *Phys. Rev. C*, 86(6):065803, 2012.
- [43] L. F. Roberts, S. E. Woosley, and R. D. Hoffman. *ApJ*, 722:954–967, 2010.
- [44] C. Sneden, J. J. Cowan, and R. Gallino. *Ann. Rev. Astron. & Astrophys.*, 46:241–288, 2008.

- [45] R. Surman and G. C. McLaughlin. *ApJ*, 603:611–623, 2004.
- [46] C. Thompson and R. C. Duncan. *ApJ*, 408:194–217, 1993.
- [47] T. A. Thompson. *ApJL*, 585:L33–L36, 2003.
- [48] T. A. Thompson, A. Burrows, and B. S. Meyer. *ApJ*, 562:887–908, 2001.
- [49] C. Travaglio, R. Gallino, E. Arnone, J. Cowan, F. Jordan, and C. Sneden. *ApJ*, 601:864–884, 2004.
- [50] J. W. Truran and J. J. Cowan. In W. Hillebrandt & E. Müller, editor, *Nuclear Astrophysics, 2000*, page 64, 2000.
- [51] S. Wanajo. *ApJL*, 770:L22, 2013.
- [52] S. Wanajo, H.-T. Janka, and S. Kubono. *ApJ*, 729:46, 2011.
- [53] S. Wanajo, H.-T. Janka, and B. Müller. *ApJL*, 726:L15, 2011.
- [54] S. Wanajo, K. Nomoto, H.-T. Janka, F. S. Kitaura, and B. Müller. *ApJ*, 695:208–220, 2009.
- [55] S. Wanajo. *ApJ*, 647:1323–1340, 2006.
- [56] J. Witti, H.-T. Janka, and K. Takahashi. *A&A*, 286:841–856, 1994.
- [57] S. E. Woosley and R. D. Hoffman. *ApJ*, 395:202–239, 1992.
- [58] S. E. Woosley, J. R. Wilson, G. J. Mathews, R. D. Hoffman, and B. S. Meyer. *ApJ*, 433:229–246, 1994.

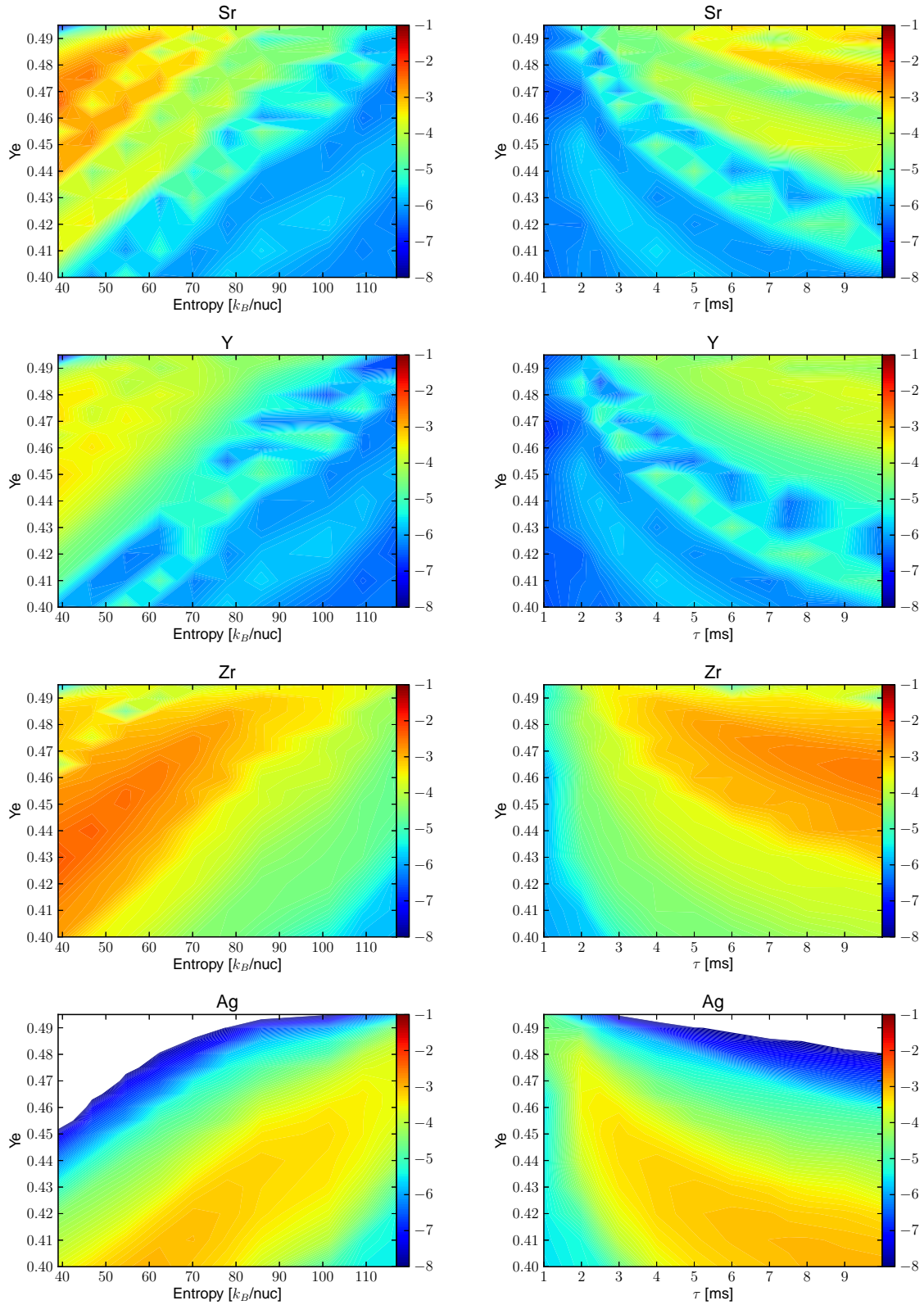


Figure 3. Color contours show the abundance in log scale of Sr, Y, Zr, and Ag from the top to the bottom for different Y_e and entropy (left column) or time scale (right column).

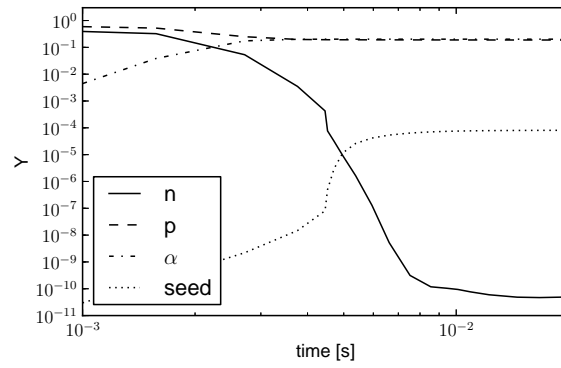


Figure 4. Abundance evolution for neutrons, protons, alpha particles, and seed nuclei in a proton-rich wind.

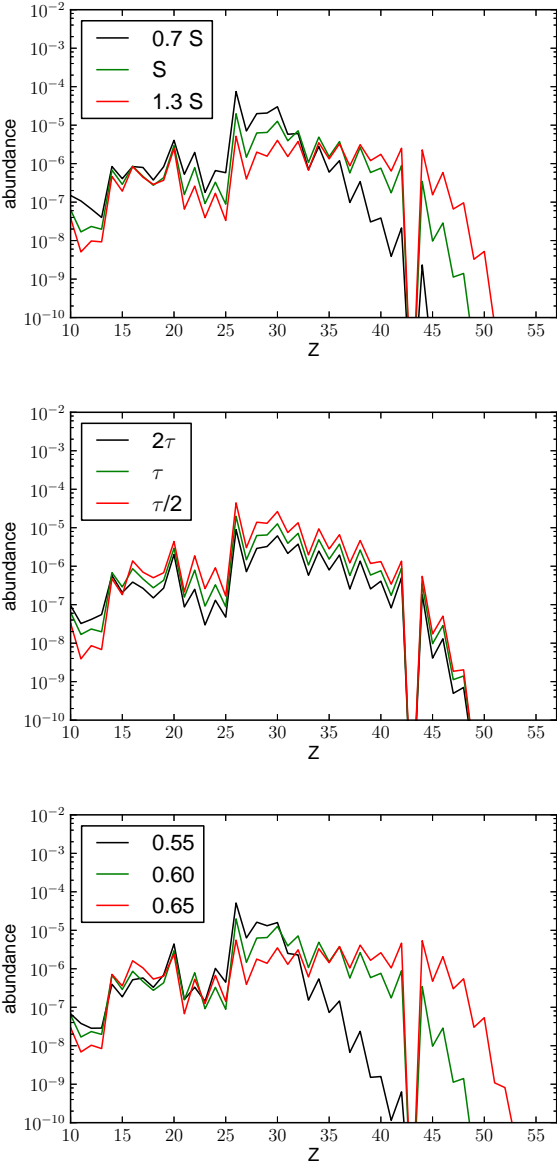


Figure 5. Elemental abundances showing the impact of entropy, expansion time scale and electron fraction, from the top to the bottom panel.

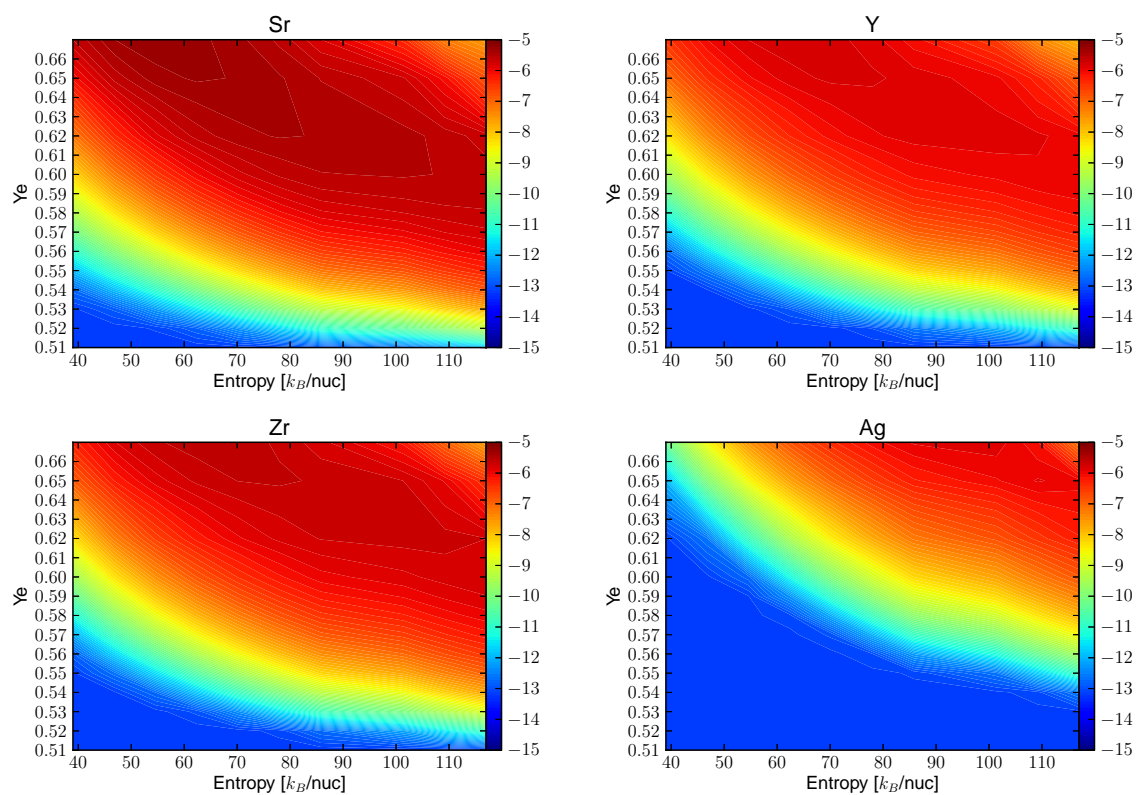


Figure 6. Color contours show the abundance in log scale of Sr, Y, Zr, and Ag for different Y_e and entropy.